

CONTEXT-AWARE META-LEARNING

Christopher Fifty¹, Dennis Duan^{1,2}, Ronald G. Junkins¹,
Ehsan Amid³, Jure Leskovec¹, Christopher Ré¹, Sebastian Thrun¹

¹Stanford University, ²Google, ³Google DeepMind
fifty@cs.stanford.com

ABSTRACT

Large Language Models like ChatGPT demonstrate a remarkable capacity to learn new concepts during inference without any fine-tuning. However, visual models trained to detect new objects during inference have been unable to replicate this ability, and instead either perform poorly or require meta-training and/or fine-tuning on similar objects. In this work, we propose a meta-learning algorithm that emulates Large Language Models by learning new visual concepts during inference without fine-tuning. Our approach leverages a frozen pre-trained feature extractor, and analogous to in-context learning, recasts meta-learning as sequence modeling over datapoints with known labels and a test datapoint with an unknown label. On 8 out of 11 meta-learning benchmarks, our approach—without meta-training or fine-tuning—exceeds or matches the state-of-the-art algorithm, P>M>F, which is meta-trained on these benchmarks.

1 INTRODUCTION

Meta-learning algorithms for image classification aim to classify a set of unlabeled images from only several labeled examples. The labeled examples are termed the *support set* and the set of unknown images is called the *query set*. In an n -way- k -shot meta-learning paradigm, the support set spans n different classes, each class contains k labeled images, and the meta-learning algorithm predicts the class of each unlabeled image in the query set from the n classes in the support set.

Nearly all meta-learning algorithms ascribe to a common pattern of pre-training, meta-training, and/or fine-tuning (Hu et al., 2022). Pre-training initializes the meta-learner’s feature extractor with a pre-trained vision model; meta-training trains the model’s parameters to learn how to classify new visual concepts during inference by training the model on a series of n -way, k -shot classification tasks; and fine-tuning updates the model’s parameters on the support set at inference.

While meta-training excels in learning new classes during inference that are similar to those seen during meta-training, it often fails to generalize to new classification paradigms. For example, models meta-trained on coarse-grained object detection often fail to generalize to fine-grained image classification. Fine-tuning on the support set during inference can rescue an otherwise poor performing model; however, training a model during inference is often impractical and prohibitive of many real-time applications. In this regard, visual meta-learning algorithms lag behind recent advancements in natural language where Large Language Models (LLMs) exhibit a remarkable capacity to learn new concepts during inference without fine-tuning (Brown et al., 2020).

In this work, we develop a meta-learning algorithm that emulates LLMs by learning new visual concepts during inference without fine-tuning. Drawing inspiration from in-context learning in LLMs, we reformulate n -way- k -shot image classification as sequence modeling over the support set and an unknown query image. This is, to the best of our knowledge, the first approach that enables in-context learning in the visual domain.

An overview of our approach is visualized in Figure 1. It first encodes support and query images with a frozen CLIP (Radford et al., 2021) model and represents support set labels with an *Equal Length and Maximally Equiangular Set* (ELMES) encoding. It then concatenates image embeddings with label embeddings to compose a joint image-label embedding and collates each embedded vector from the query and support set into a sequence. We then pre-train a sequence model—in our experiments a Transformer encoder—across several large datasets with an explicit in-context learning objective:

classify the query given an input sequence composed of the support set and query point. This learning paradigm trains the Transformer encoder to extrapolate to new classes in the parameter-space of the model, enabling our approach to learn new visual concepts during inference without fine-tuning. Due to its capacity to learn visual information “in-context”, we term our approach *Context-Aware Meta-Learning* (CAML).

Our primary contribution is to develop a meta-learning algorithm for *universal meta-learning*: the capacity to learn any new visual concept during inference without fine-tuning or meta-training on related images. This challenging setting emulates the deployment of LLMs to real-time applications, and strong performance in this setting would unlock new applications of visual meta-learning. Our theoretical analysis shows that an ELMES is the encoding that minimizes the entropy of detecting classes within the support set, and therefore, does not need to be learned. Our empirical analysis highlights the importance of reformulating meta-learning as sequence modeling: considering the support set and query together enables the model to attend to specific visual features of images in the support set to classify the query. Finally, our empirical analysis indicates CAML is a state-of-the-art meta-learning algorithm. On a diverse set of 8 out of 11 meta-learning benchmarks—and without meta-training or fine-tuning—CAML outperforms or matches the performance of P>M>F (Hu et al., 2022), a state-of-the-art meta-learning algorithm that is meta-trained on each benchmark.

2 RELATED WORK

Meta-Learning Algorithms. Many recent meta-learning algorithms can be categorized as either *gradient-based* or *metric-based* (Bouniot et al., 2022); however, CAML belongs to a new category of *context-based* methods that casts meta-learning as learning over a sequence composed of the query and support set to predict the label of the query (Fifty et al., 2023). Dissimilar from other *context-based* methods, CAML avoids meta-training and can generalize to out-of-distribution classes during inference.

Gradient-based algorithms learn representations during meta-training that can be quickly adapted to new data distributions by fine-tuning on the support set (Chen et al., 2020b; Finn et al., 2017; Nichol & Schulman, 2018; Bertinetto et al., 2018a; Lee et al., 2019a; Nichol et al., 2018; Raghu et al., 2019). Dissimilar from *context-based* algorithms, they require fine-tuning during inference, and this property makes them unsuitable for real-time applications. *Metric-based* algorithms learn a distance-sensitive embedding space during meta-training, and during inference, the query is classified by its distance to points in the support set (Allen et al., 2019; Li et al., 2019a; Simon et al., 2020; Snell et al., 2017a; Sung et al., 2018). While *metric-based* algorithms do not require fine-tuning during inference, they often exhibit poor performance when encountering classes during inference that are significantly different from those seen during meta-training (Hu et al., 2022).

Cross-Domain Meta-Learning. Cross-domain meta-learning refers to a challenging evaluation paradigm where the meta-training and inference-time data distributions are significantly different (Chen et al., 2019). Recent work finds that leveraging self-supervised pre-training—or foundational model feature extractors—can significantly improve cross-domain performance (Hu et al., 2022; Zhang et al., 2021). Moreover, fine-tuning with respect to the support set almost always outperforms meta-learning without fine-tuning in this setting (Guo et al., 2020; Oh et al., 2022; Phoo & Hariharan, 2020; Islam et al., 2021). While effective, fine-tuning is prohibitive to deploying visual meta-learning models in a manner similar to LLMs like ChatGPT as the latency and memory cost to fine-tune a model’s parameters on each user query is untenable. Moreover, fine-tuning is sensitive to the choice of learning rate, making these models difficult to deploy in practice (Hu et al., 2022).

3 APPROACH

We adapt the ideas underpinning in-context learning in LLMs—namely learning to classify a query from a context of support set demonstrations in a single forward pass—to image classification. A similar concept has recently been explored by Fifty et al. (2023) for few-shot molecular property prediction. Dissimilar from this work, we avoid meta-training and instead focus on universal image classification: learning to detect new visual classes during inference without meta-training on related classes or fine-tuning on the support set.

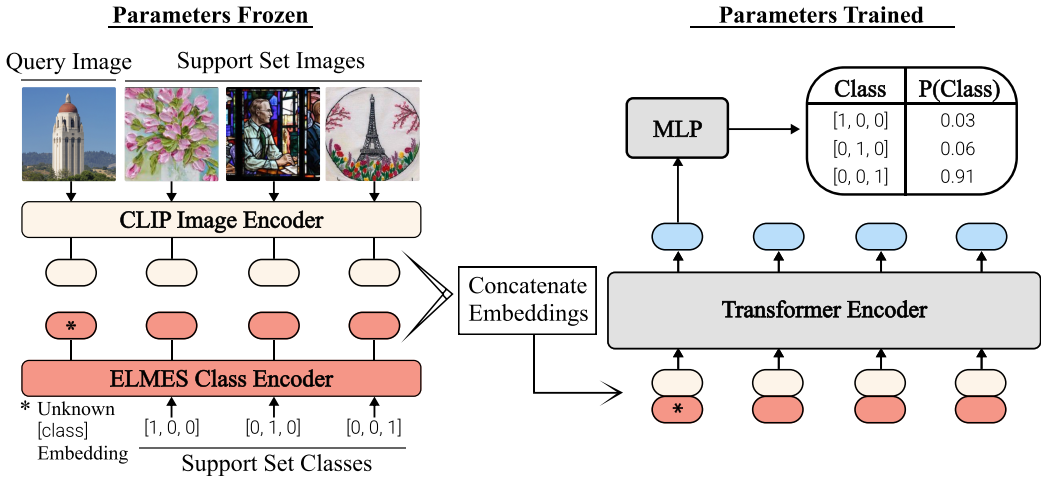


Figure 1: Overview of **CAML**. Query and support set images are encoded with a CLIP feature extractor and then concatenated with their corresponding ELMES label embeddings. We feed the resulting sequence of concatenated vectors into a Transformer encoder and extract the transformed query vector from the output sequence to predict its class.

Architecture. **CAML** consists of three components: (1) a frozen CLIP image encoder, (2) a fixed ELMES class encoder, and (3) a Transformer encoder sequence model. **CAML** first encodes query and support set images using a frozen CLIP feature extractor. Crucially, the CLIP embedding space distills images into low-dimensional representations so that images with similar visual characteristics and semantic meanings have similar embeddings. We encode the classes of the support set with an ELMES class encoder. In Section 4, we prove that an ELMES encoding of mutually exclusive labels allows the Transformer encoder sequence model to maximally identify classes within the support set. As the class of the query is unknown, it uses a special learnable “unknown token” embedding.

The core idea underpinning **CAML** is to cast meta-learning as sequence modeling over the support set and query points. We instantiate the sequence model as a Transformer encoder, and during large-scale pre-training, train the model to predict the class of the query from an input sequence composed of the support set and query embedded vectors. Specifically, the input to the Transformer encoder is a sequence of support set and query vectors embedded in the joint image-label embedding space. From the output sequence of the Transformer encoder, we select the element at the same position as the query in the input sequence, and pass this vector through a shallow MLP to predict the label of the query. A visual depiction of **CAML** is shown in Figure 1.

Large-Scale Pre-Training. As our focus is universal meta-learning—and **CAML** may encounter any new visual concept during inference—we pre-train **CAML**’s Transformer encoder on few-shot image classification tasks from ImageNet-1k (Deng et al., 2009), Fungi (Schroeder & Cui, 2018), MSCOCO (Lin et al., 2014), and WikiArt (Saleh & Elgammal, 2015). We chose these datasets because they span generic object recognition (ImageNet-1k, MSCOCO), fine-grained image classification (Fungi), and unnatural image classification (WikiArt). To avoid distorting the CLIP embedding space, we freeze the CLIP feature extractor and only update the Transformer encoder during pretraining. Similarly, since an ELMES minimizes the entropy of detecting classes within the support set, the label encoder is also frozen. In the context of pre-training, meta-training, and fine-tuning, **CAML** only requires pre-training and avoids meta-training on the train/validation splits of meta-learning benchmarks or fine-tuning on the support set during inference.

4 THEORETICAL ANALYSIS

In this section, we explore the symmetries inherent in **CAML**. These symmetries allow us to formulate the problem of learning support set class representations as an entropy minimization problem with a closed-form solution. We prove that this solution is an ELMES. Later, we show it maintains permutation invariance, a vital property of meta-learning algorithms that conveys consistent predictions irrespective of the ordering of elements within the sequence. Due to space constraints, all proofs and many definitions, properties, lemmas, and theorems are allocated to the Appendix.

4.1 EQUAL LENGTH AND MAXIMALLY EQUIANGULAR SET OF VECTORS

Definition 1. An *Equal Length and Maximally Equiangular Set (ELMES)* is a set of non-zero vectors $\{\phi_j\}_{j=1}^d$, $\phi_j \in \mathbb{R}^{d+k}$ for some $k \geq 0$ and $d > 1$, such that $\forall j \neq j'$, $\|\phi_j\| = \|\phi_{j'}\|$ and $\langle \phi_j, \phi_{j'} \rangle = \frac{-1}{d-1}$. Simply, all vectors in this set are equal length and maximally equiangular.

An *Equal Angle and Maximally Equiangular Set (ELMES)* of vectors has connections to both Equiangular Tight Frames in representation theory (Welch, 1974; Fickus et al., 2018) as well as the Simplex Equiangular Tight Frames highlighted in recent neural collapse works exploring softmax-layer geometry at the terminal phase of training (Papayan et al., 2020; Yang et al., 2022). We offer additional discussion comparing these structures in the Appendix as well as provide an intuitive view of an ELMES as a regular d -simplex immersed in \mathbb{R}^{d+k} .

4.2 LABEL SYMMETRY

Symmetry in the assignment of support classes to numeric labels is an important property of meta-learning algorithms. For example, if we have the support set classes $\{\text{tower}, \text{bear}, \text{tree}\}$, the mapping of $\{\text{bear} \rightarrow 1, \text{tower} \rightarrow 2, \text{tree} \rightarrow 3\}$ should produce the same prediction for a query point as a different mapping $\{\text{bear} \rightarrow 2, \text{tower} \rightarrow 3, \text{tree} \rightarrow 1\}$. To explore this symmetry, we examine how class embeddings are being used by the model.

From our formulation in Section 3, we represent a demonstration vector as a concatenation of an image embedding ρ and a label embedding ϕ : $[\rho \mid \phi]$. This vector is directly fed into the self-attention mechanism, where we matrix multiply with key, query, and value self-attention heads. Taking only one of these matrices for simplicity with head-dimension k :

$$[\rho \mid \phi] \begin{bmatrix} \Gamma_1 & \dots & \Gamma_k \\ \psi_1 & \dots & \psi_k \end{bmatrix} = [\langle \rho, \Gamma_1 \rangle \quad \dots \quad \langle \rho, \Gamma_k \rangle] + [\langle \phi, \psi_1 \rangle \quad \dots \quad \langle \phi, \psi_k \rangle] \quad (1)$$

The output of this transformation will be the sum of two vectors: one composed of the inner products between the image embedding and the learnable $\{\Gamma_i\}_{i=1}^k$ s and the other composed of the class embedding and the learnable $\{\psi_i\}_{i=1}^k$.

We postulate a capacity to distinguish among the classes of demonstration vectors is necessary for the model to predict the class of the query vector. Conversely, if a meta-learning algorithm predicts among d classes, and all classes maintain the same embedding $\phi_j = \phi_i \forall i \in \{1, \dots, d\}$, the model will be unable to identify the class of the query vector as all demonstration vectors appear to have the same class identity. Such an embedding would maximize the Shannon entropy for any learnable ψ_i

$$H_i(X) := - \sum_{x \in \mathcal{X}} p_i(x) \ln(p_i(x))$$

where we define $\mathcal{X} = \{1, 2, \dots, d\}$ to be the different classes, X to be a random variable which takes on values in \mathcal{X} , and $p_i(X = j) = \frac{e^{\langle \psi_i, \phi_j \rangle}}{\sum_{\ell \in \mathcal{X}} e^{\langle \psi_i, \phi_\ell \rangle}}$ as the softmax probability of class j given that ψ_i is learned to detect class i (i.e. maximize $p_i(X = i)$ and minimize $H_i(X)$).

Contrary to the above example, we assume a capacity to learn a ψ_i that maximally detects a given class j will be beneficial to minimizing the loss for meta-learning paradigms. As we use the softmax of the inner product to determine class probabilities, maximizing $p_i(X = j)$ is equivalent to minimizing $p_i(X = \ell)$ for all $\ell \neq j$.

By symmetry in the assignment of class embeddings to support classes, we can assume that the number of ψ_i learned to detect class i is similar to the number of ψ_j learned to detect class j for all pairs (i, j) . Then $p_i(X = i)$ for all $1 \leq i \leq d$ is jointly maximized \iff the d -class embeddings $\{\phi_j\}_{j=1}^d$ is an ELMES. Before we prove this result, we leverage symmetry in the assignment of labels to classes to make the following assumptions (justifications for each assumption located in the Appendix):

Assumption 1. Suppose $\{\psi_i\}_{i=1}^k$ are learnable class detectors of unit norm with at least one ψ_i detecting each class $1 \leq i \leq d$. The probability $p_j(X = j) = p_i(X = i)$ for $1 \leq i, j \leq d$.

Assumption 2. Define $p_i(X = i) \setminus \{\phi_l\}_{l=(m+1)}^d$ as the probability of ψ_i detecting ϕ_i from the set of vectors $\{\phi_j\}_{j=1}^m$, $m < d$. Then the probability $p_j(X = j) \setminus \{\phi_l\}_{l=(m+1)}^d = p_i(X = i) \setminus \{\phi_l\}_{l=(m+1)}^d$ for $1 \leq i, j \leq m$ and $m \geq 2$.

Assumption 3. When $\psi_i = \frac{\phi_i}{\|\phi_i\|}$, $p_i(X = i)$ is maximized.

When Assumption 1, Assumption 2, and Assumption 3 hold, the set of class embeddings that maximize the probability of a learnable ψ_i detecting class i is necessarily an ELMES.

Theorem 1. The set of class embeddings $\{\phi_j\}_{j=1}^d \forall j, 1 \leq j \leq d$ that maximizes $p_j(X = j)$ is necessarily an ELMES.

Alternatively when viewed through the lens of information theory, we can reinterpret an ELMES as the class embedding that minimizes the entropy of ψ_i detecting class i . Informally, ELMES causes ψ_i to have the least uncertainty when detecting class i .

Lemma 1. Let H_i be the entropy of $p_i(X)$. An ELMES minimizes H_i .

4.3 PERMUTATION INVARIANCE.

In addition to label symmetry, it is also desirable for the output prediction of **CAML** to not depend on the order of demonstrations in the sequence. As [Fifty et al. \(2023\)](#) show that a two-class, non-ELMES version of **CAML** is invariant to permutations in the input sequence, it suffices to show that the ELMES label encoder is equivariant to permutations in the input sequence.

Lemma 2. Consider a n -sequence of one-hot labels stacked into a matrix $S \in \mathbb{R}^{n \times w}$, and an ELMES label encoder denoted by $W \in \mathbb{R}^{w \times d}$ with w denoting “way” and d the dimension of the label embedding. The label embedding SW is equivariant to permutations.

5 EXPERIMENTS

To quantify universal image classification performance, we evaluate a diverse set of 11 meta-learning benchmarks divided across 4 different categories:

1. Generic Object Recognition: mini-ImageNet ([Vinyals et al., 2016](#)), tiered-ImageNet ([Ren et al., 2018](#)), CIFAR-fs ([Bertinetto et al., 2018b](#)), and Pascal VOC ([Everingham et al.](#))
2. Fine-Grained Image Classification: CUB ([Wah et al., 2011](#)), Aircraft ([Maji et al., 2013](#)), meta-iNat ([Wertheimer & Hariharan, 2019](#)), and tiered meta-iNat ([Wertheimer & Hariharan, 2019](#))
3. Unnatural Image Classification: ChestX ([Guo et al., 2020](#)) and Paintings ([Crowley & Zisserman, 2015](#))
4. Inter-Domain Image Classification: Pascal+Paintings ([Everingham et al.; Crowley & Zisserman, 2015](#)).

Generic object recognition, fine-grained image classification, and unnatural image classification are standard benchmarking tasks in meta-learning literature ([Chen et al., 2020a](#); [Hu et al., 2022](#); [Wertheimer et al., 2020](#); [Guo et al., 2020](#)). Beyond this, we compose a challenging new *inter-domain* category by combining Pascal VOC with Paintings so that each class is composed of both natural images and paintings. This allows us to evaluate the ability of meta-learning algorithms to generalize across domains within the same class. For example, the support image for the class “tower” may be Van Gogh’s *The Starry Night*, while the query may be a picture of the Eiffel Tower. Humans have the ability to generalize visual concepts between such domains; however, meta-learning algorithms struggle with this formulation ([Jankowski & Grąbczewski, 2011](#)).

5.1 BASELINES

We evaluate the capacity of **CAML**, Prototypical Networks ([Snell et al., 2017b](#)), MetaOpt ([Lee et al., 2019b](#)), and MetaQDA ([Zhang et al., 2021](#)) in a universal meta-learning setting by pre-training them with the same CLIP feature extractor over the same image corpus as **CAML** and similarly freezing their weights at inference time. We select Prototypical Networks and MetaOpt as baselines as they are well-studied and have been shown to perform well with a pre-trained foundational model feature extractor ([Hu et al., 2022](#)). Similarly, MetaQDA benefits from pre-trained feature extractors and was designed for cross-domain meta-learning ([Zhang et al., 2021](#); [Hu et al., 2022](#)).

To assess the performance gap between universal meta-learning and the typical meta-training approach, we also benchmark the performance of the current state-of-the-art meta-learning algorithm,

Table 1: **MiniImageNet & CIFAR-fs** mean accuracy and standard error comparison with representative state-of-the-art meta-learning algorithms. Methods using external data during pre-training are indicated. † indicates the ViT-base CLIP backbone was frozen during pre-training.

Method (Backbone)	Extra Data	CIFAR-fs		MiniImageNet	
		5w-1s	5w-5s	5w-1s	5w-5s
Inductive					
ProtoNet (CNN-4-64) (Snell et al., 2017b)		49.4	68.2	55.5	72.0
Baseline++ (CN-4-64) (Chen et al., 2020a)				61.4	77.9
MetaOpt (ResNet12) (Lee et al., 2019b)		72.0	84.3	61.4	77.9
Meta-Baseline (ResNet12) (Chen et al., 2021b)		68.6	83.7		
MetaQDA (WRN-28-10) (Zhang et al., 2021)	✓	74.3	89.6	67.8	84.3
RankDNN (ResNet12)(Guo et al., 2022)		78.9	90.6	66.7	84.8
PatchProto+TSF (WRN-28) (Lai et al., 2022)				70.2	84.6
P>M>F (ViT-base) Hu et al. (2022)	✓	84.3	92.2	95.3	98.4
Transductive					
Fine-tuning (WRN-28-10) (Dhillon et al., 2020)		76.6	85.8	65.7	78.4
SIB (WRN-28-10) (Hu et al., 2020)		80.0	85.3	70.0	79.2
PT-MAP (WRN-28-10) (Hu et al., 2021)		87.7	90.7	82.9	88.8
CNAPS (ResNet18) (Bateni et al., 2021)	✓			79.9	88.1
Self-supervised					
ProtoNet (WRN-28-10) (Gidaris et al., 2019)		73.6	86.1	62.9	79.9
ProtoNet (AMDIM ResNet) (Chen et al., 2021a)	✓			76.8	91.0
EPNet + SSL (WRN-28-10) (Rodríguez et al., 2020)	✓			79.2	88.1
Semi-supervised					
LST (ResNet12) (Li et al., 2019b)	✓			70.1	78.7
PLCM (ResNet12) (Huang et al., 2021)	✓	77.6	86.1	70.1	83.7
Universal Meta-Learning; No Meta-Training or Finetuning					
ProtoNet (ViT-base) (Snell et al., 2017b)	✓	62.9±.2	79.7±.2	92.1±.1	97.1±.0
ProtoNet (ViT-base)†	✓	57.7±.2	81.0±.2	85.3±.2	96.0±.1
MetaOpt (ViT-base) (Lee et al., 2019b)	✓	53.1±.3	73.1±.2	78.5±.2	91.6±.1
MetaOpt (ViT-base)†	✓	61.7±.2	83.1±.1	86.9±.2	96.5±.1
MetaQDA (ViT-base) (Zhang et al., 2021)	✓	60.4±.2	83.2±.1	88.2±.2	97.4±.0
CAML (ViT-base)	✓	70.8±.2	85.5±.1	96.2±.1	98.6±.0

Table 2: **Pascal & Paintings** mean accuracy and standard error across 10,000 test epochs. † indicates the ViT-base CLIP backbone was frozen during pre-training.

Method (Backbone)	Pascal + Paintings		Paintings		Pascal	
	5w-1s	5w-5s	5w-1s	5w-5s	5w-1s	5w-5s
In-Domain [Meta-Training]						
P>M>F (ViT-base)	60.7	74.4	53.2	65.8	72.2	84.4
Universal Meta-Learning						
ProtoNet (ViT-base)	49.6±.2	63.5±.1	38.3±.2	48.2±.1	77.9±.2	87.3±.2
ProtoNet (ViT-base)†	52.2±.2	70.6±.1	48.3±.2	64.1±.1	72.2±.2	84.3±.2
MetaOpt (ViT-base)	38.2±.2	58.2±.1	31.6±.2	48.0±.1	63.7±.2	81.7±.2
MetaOpt (ViT-base)†	53.2±.2	74.8±.1	49.3±.2	65.9±.1	72.8±.2	84.4±.2
MetaQDA (ViT-base)	53.8±.2	74.1±.1	49.4±.2	66.6±.1	73.5±.2	85.2±.2
CAML (ViT-base)	63.8±.2	78.3±.1	51.1±.2	65.2±.1	82.6±.2	89.7±.1

P>M>F (Hu et al., 2022), which is meta-trained on each dataset. While previous cross-domain approaches often involve fine-tuning on the support set at inference time, we forgo this step as fine-tuning is incompatible with universal meta-learning and developing real-time meta-learning applications.

When pre-training all models in the universal meta-learning setting, we set the learning rate to a fixed 1×10^{-5} and do not perform any hyperparameter tuning in order to match the practices used by P>M>F. We use early stopping with a window size of 10 epochs during pre-training and the code

Table 3: **meta-iNat & tiered meta-iNat & ChestX** mean accuracy and standard error across 10,000 test epochs. † indicates the ViT-base CLIP backbone was frozen during pre-training.

Method (Backbone)	meta-iNat		tiered meta-iNat		ChestX	
	5w-1s	5w-5s	5w-1s	5w-5s	5w-1s	5w-5s
In-Domain [Meta-Training]						
P>M>F (ViT-base)	91.2	96.1	74.8	89.9	27.0	32.1
Universal Meta-Learning						
ProtoNet (ViT-base)	78.4±.2	89.4±.1	66.3±.2	82.2±.2	22.4±.1	25.3±.1
ProtoNet (ViT-base)†	84.5±.2	94.8±.1	73.8±.2	89.5±.1	22.7±.1	25.8±.1
MetaOpt (ViT-base)	53.0±.2	77.7±.2	37.3±.2	63.0±.2	20.8±.1	23.0±.1
MetaOpt (ViT-base)†	85.5±.2	95.5±.1	75.1±.2	91.9±.1	23.0±.1	27.4±.1
MetaQDA (ViT-base)	86.3±.2	95.9±.1	76.0±.2	92.4±.1	22.6±.1	27.0±.1
CAML (ViT-base)	91.2±.2	96.3±.1	81.9±.2	91.6±.1	21.5±.1	22.2±.1

Table 4: **CUB & tiered-ImageNet & Aircraft** mean accuracy and standard error across 10,000 test epochs. † indicates the ViT-base CLIP backbone was frozen during pre-training.

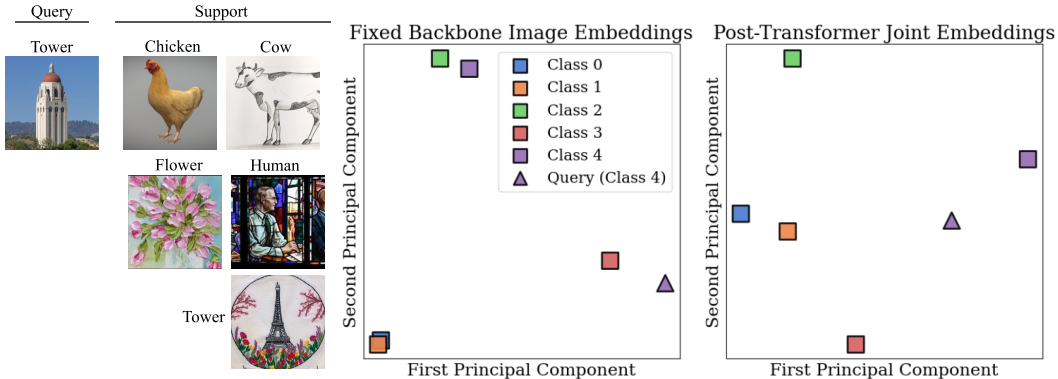
Method (Backbone)	CUB		tiered-ImageNet		Aircraft	
	5w-1s	5w-5s	5w-1s	5w-5s	5w-1s	5w-5s
In-Domain [Meta-Training]						
P>M>F (ViT-base)	92.3	97.0	93.5	97.3	79.8	89.3
Universal Meta-Learning						
ProtoNet (ViT-base)	59.4±.2	77.3±.2	93.5±.1	97.4±.1	37.9±.2	52.5±.2
ProtoNet (ViT-base)†	87.0±.2	97.1±.1	87.3±.2	96.1±.1	62.4±.3	82.0±.2
MetaOpt (ViT-base)	71.5±.2	41.2±.2	76.6±.2	89.6±.1	41.6±.2	26.7±.1
MetaOpt (ViT-base)†	87.9±.2	97.2±.1	88.2±.2	96.5±.1	64.8±.2	82.6±.2
MetaQDA (ViT-base)	88.3±.2	97.4±.1	89.4±.2	97.0±.1	63.6±.3	83.0±.2
CAML (ViT-base)	91.8±.2	97.1±.1	95.4±.1	98.1±.1	63.3±.3	79.1±.2

release of [Hu et al. \(2022\)](#) to benchmark P>M>F with the training settings and hyperparameters described in their work.

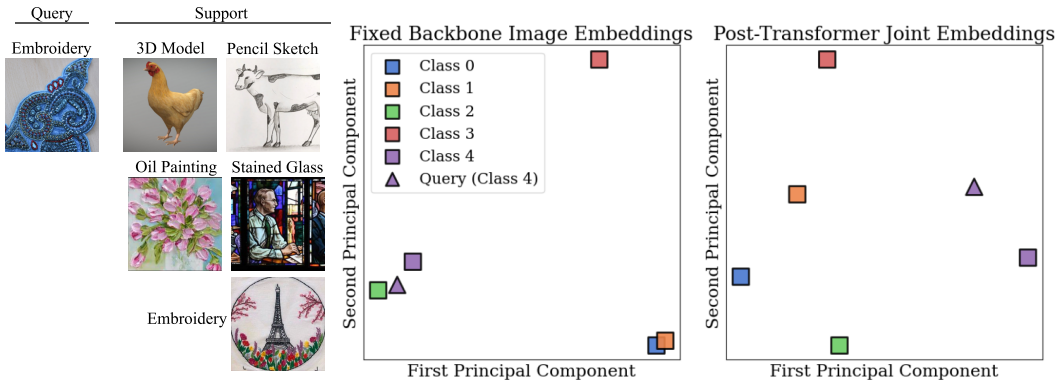
5.2 RESULTS

Our findings are summarized in Table 1, Table 2, Table 3, and Table 4 and indicate that **CAML** sets a new state-of-the-art for universal meta-learning by significantly outperforming other baselines on 15 of 22 evaluation settings. For 5 of the other 7 evaluation settings, **CAML** matches—or nearly matches—the best performing baseline. Remarkably, **CAML** also performs competitively with P>M>F on 8 out of 11 meta-learning benchmarks, even though P>M>F meta-trains on the training set of each benchmark. This result suggests that the amount of new visual information learned during inference when using only foundational models and novel meta-learning techniques without fine-tuning is comparable to the amount learned when directly meta-training on in-domain data. This capacity may unlock new applications in the visual space, just as the emergence of in-context learning in LLMs has enabled many new applications in natural language.

The 3 datasets where P>M>F outperforms **CAML** are CIFAR-fs, Aircraft, and ChestX. CIFAR-fs is a generic object recognition benchmark containing CIFAR images downsampled to 32x32 resolution. As **CAML** and CLIP pre-train on 224x224 resolution images, downsampling by a factor of 49 likely induces a distribution shift that was not learned by **CAML** during large-scale pre-training. In the cases of Aircraft and ChestX, we postulate that the CLIP embedding space—structured so images with similar captions have similar embeddings—struggles to effectively differentiate between the fine-grained, specialized classes in these tasks. For example, while a Boeing 737 and Airbus A380 have different labels in the Aircraft dataset, the scraped CLIP captions for those images may not reach that level of granularity. This corroborates the findings from [Radford et al. \(2021\)](#), which found that in a zero-shot setting, CLIP underperforms in specialized or complex tasks such as medical imaging or aircraft classification. We anticipate the continued development of visual (or multi-modal)



(a) Left: An example task, classifying images by the objects depicted. Center: CLIP image embeddings on this task’s images. Right: joint image+label representations after the last CAML attention layer for the same task.



(b) Left: An example task, classifying images by the artistic medium used. Center: CLIP image embeddings on this task’s images. Right: joint representations after the last CAML attention layer for the same task.

Figure 2: Two sample tasks over the same support images but utilizing different criteria to define classes. The nature of the query image informs the task being presented, e.g. classification by object (top) vs. classification by texture (bottom). For both, the final-layer attention outputs provide better separation between class representations and groups the query representation with the proper task, even when projected into 2D space by PCA.

foundational models will improve their sensitivity to fine-grained visual concepts and significantly increase the performance of CAML on these benchmarks.

Finally, our empirical findings indicate that large-scale pre-training often decreases the performance of Prototypical Networks and MetaOpt. We observe that these methods tend to overfit during pre-training, and our empirical results show a similar pattern: pre-training with these methods often helps the performance of benchmarks similar to ImageNet (i.e. Pascal, MiniImageNet, tiered-ImageNet), but it significantly hurts the performance of out-of-domain tasks (i.e. Aircraft, CUB, Paintings) as shown in Tables 1 to 4. We believe large-scale pre-training of the CLIP backbone distorts the structure of the CLIP embedding space, leading to catastrophic forgetting on out-of-domain tasks. Conversely, CAML and MetaQDA—both of which freeze the parameters of the CLIP feature extractor—benefit greatly from large-scale pre-training. With the increasing scale and sophistication of visual feature extractors, fine-tuning—or even loading these models into memory—becomes less feasible. Algorithms that do not fine-tune this backbone like CAML and MetaQDA will benefit from this research and likely become even more effective.

5.3 WEAKNESSES OF CAML

Despite its strong empirical performance, CAML presents several weaknesses. First, the maximum number of classes present in the support set at any point during inference must be known at pre-training to instantiate a d -way ELMES. Further, at least one dataset during pre-training must use a

d -way classification setting so the ψ_i class detectors referenced in Section 4 are trained within the Transformer encoder’s attention layers. Another weakness relates to reliance on the frozen image encoder. As **CAML** does not update these parameters at all, it can underperform on tasks that are difficult to distinguish or highly spread out in the CLIP embedding space, such as low-resolution images or specialized fine-grained classes.

6 ANALYSIS

To better understand how **CAML** learns, we conduct empirical analyses on (1) its ability to dynamically update its representations at inference time, and (2) the effect of the fixed ELMES class embedding.

Context-Aware Representations. Dissimilar from other meta-learning algorithms and due to recasting meta-learning as sequence modeling, **CAML** considers the full context of a query and support set to predict the label of the query. Specifically, the query dynamically influences the representation of support set points, and the support set points dynamically influence the representation of the query as this sequence is passed through the layers of a Transformer encoder. This property enables universal meta-learning by allowing the model to update the support and query representations based on the context of the task, not only the contents of the images.

An example where the query dynamically influences the support set is visualized in Figure 2. Given only the 5 support examples, the prediction task is ambiguous. However, the nature of the query determines the prediction task. The query image of a tower in Figure 2a reduces the task to generic object recognition: classify the query based on the object portrayed in the image. On the other hand, and as visualized in Figure 2b, the query image of embroidery reduces the prediction task to texture identification: classify the query based on artistic medium.

To analyze how dynamic representations affect **CAML**, we examine the representations of the support set and query vectors at the input to and output of the Transformer encoder. For both examples visualized in Figure 2a and Figure 2b, the Transformer encoder learns to separate support set vectors by class identity, and moreover, group the query representation with the correct support set example.

We find the frozen CLIP image embeddings are actually antagonistic for the classification-by-texture task visualized in Figure 2b: the query image embedding is closest to the support set example for the second class, “oil painting”. Moreover, we find that our baseline methods that rely on frozen CLIP image embeddings like MetaQDA, ProtoNet[†], and MetaOpt[†] group the query with “oil painting” and therefore misclassify this example. On the other hand, as **CAML** considers the full context of the query and support set, it develops representations of the query in the context of the support set—and the support set in the context of the query—to group the query with the “embroidery” support set image as they share the same texture, thereby correctly classifying this example.

ELMES Ablation. To supplement our theoretical analysis in Section 4, we train a version of **CAML** with learnable class embedding vectors in place of the fixed ELMES encoder. Given our analysis in Section 4, it is perhaps unsurprising we find that—without any constraints or limitations—the class embeddings converge to an ELMES. The average pair-wise angle between embedding vectors is 1.77 ± 0.02 radians whereas the expected pairwise angle from an ELMES is 1.82. Similarly, the average norm of the learnable class embeddings converges to 1.34 ± 0.02 whereas the learned norm of the ELMES model is 1.32.

An evaluation comparing **CAML** with learnable class embeddings to the approach with a fixed ELMES encoder is presented in Table 5, Table 6, Table 7, and Table 8 of the Appendix. In summary, the performance is approximately the same on each benchmark with the exception of Aircraft. In this case, the learnable embedding model significantly outperforms the ELMES model, and moreover, surpasses all other universal meta-learning baselines on the 5-way-1-shot split with an accuracy of $66.3 \pm .2$. Nevertheless, given the similarity between both approaches on the remaining 10 datasets, and the learnable class embeddings actually forming an ELMES, we attribute the difference in Aircraft performance to stochasticity in training the model, suggesting that the fixed ELMES encoder is indeed optimal.

7 CONCLUSION

In this work, we develop **CAML**, a meta-learning algorithm that emulates in-context learning in LLMs by learning new visual concepts during inference without fine-tuning. Our empirical findings show that **CAML**—without meta-training or fine-tuning—exceeds or matches the performance of the current state-of-the-art meta-learning algorithm on 8 out of 11 benchmarks. This result indicates visual meta-learning models are ready for deployment in a manner similar to LLMs, and we hope this work recalibrates our sense of limitations for the universal meta-learning paradigm.

REFERENCES

- Kelsey Allen, Evan Shelhamer, Hanul Shin, and Joshua Tenenbaum. Infinite mixture prototypes for few-shot learning. In *International conference on machine learning*, pp. 232–241. PMLR, 2019.
- Peyman Bateni, Jarred Barber, Jan-Willem van de Meent, and Frank Wood. Enhancing few-shot image classification with unlabelled examples, 2021.
- Luca Bertinetto, Joao F Henriques, Philip HS Torr, and Andrea Vedaldi. Meta-learning with differentiable closed-form solvers. *arXiv preprint arXiv:1805.08136*, 2018a.
- Luca Bertinetto, Joao F Henriques, Philip HS Torr, and Andrea Vedaldi. Meta-learning with differentiable closed-form solvers. *arXiv preprint arXiv:1805.08136*, 2018b.
- Quentin Bouniot, Ievgen Redko, Romaric Audigier, Angélique Loesch, and Amaury Habrard. Improving few-shot learning through multi-task representation learning theory. In *European Conference on Computer Vision*, pp. 435–452. Springer, 2022.
- Tom Brown, Benjamin Mann, Nick Ryder, Melanie Subbiah, Jared D Kaplan, Prafulla Dhariwal, Arvind Neelakantan, Pranav Shyam, Girish Sastry, Amanda Askell, et al. Language models are few-shot learners. *Advances in neural information processing systems*, 33:1877–1901, 2020.
- Da Chen, Yuefeng Chen, Yuhong Li, Feng Mao, Yuan He, and Hui Xue. Self-supervised learning for few-shot image classification, 2021a.
- Wei-Yu Chen, Yen-Cheng Liu, Zsolt Kira, Yu-Chiang Frank Wang, and Jia-Bin Huang. A closer look at few-shot classification. *arXiv preprint arXiv:1904.04232*, 2019.
- Wei-Yu Chen, Yen-Cheng Liu, Zsolt Kira, Yu-Chiang Frank Wang, and Jia-Bin Huang. A closer look at few-shot classification, 2020a.
- Xiaohan Chen, Zhangyang Wang, Siyu Tang, and Krikamol Muandet. Mate: plugging in model awareness to task embedding for meta learning. *Advances in neural information processing systems*, 33:11865–11877, 2020b.
- Yinbo Chen, Zhuang Liu, Huijuan Xu, Trevor Darrell, and Xiaolong Wang. Meta-baseline: Exploring simple meta-learning for few-shot learning, 2021b.
- Elliot J Crowley and Andrew Zisserman. In search of art. In *Computer Vision-ECCV 2014 Workshops: Zurich, Switzerland, September 6-7 and 12, 2014, Proceedings, Part I 13*, pp. 54–70. Springer, 2015.
- Jia Deng, Wei Dong, Richard Socher, Li-Jia Li, Kai Li, and Li Fei-Fei. Imagenet: A large-scale hierarchical image database. In *2009 IEEE Conference on Computer Vision and Pattern Recognition*, pp. 248–255, 2009. doi: 10.1109/CVPR.2009.5206848.
- Guneet S. Dhillon, Pratik Chaudhari, Avinash Ravichandran, and Stefano Soatto. A baseline for few-shot image classification, 2020.
- M. Everingham, L. Van Gool, C. K. I. Williams, J. Winn, and A. Zisserman. The PASCAL Visual Object Classes Challenge 2012 (VOC2012) Results. <http://www.pascal-network.org/challenges/VOC/voc2012/workshop/index.html>.

- Matthew Fickus, John Jasper, Emily J King, and Dustin G Mixon. Equiangular tight frames that contain regular simplices. *Linear Algebra and its applications*, 555:98–138, 2018.
- Christopher Fifty, Jure Leskovec, and Sebastian Thrun. In-context learning for few-shot molecular property prediction, 2023.
- Chelsea Finn, Pieter Abbeel, and Sergey Levine. Model-agnostic meta-learning for fast adaptation of deep networks. In *International conference on machine learning*, pp. 1126–1135. PMLR, 2017.
- Spyros Gidaris, Andrei Bursuc, Nikos Komodakis, Patrick Pérez, and Matthieu Cord. Boosting few-shot visual learning with self-supervision, 2019.
- Qianyu Guo, Hongtong Gong, Xujun Wei, Yanwei Fu, Weifeng Ge, Yizhou Yu, and Wenqiang Zhang. Rankdnn: Learning to rank for few-shot learning, 2022.
- Yunhui Guo, Noel C Codella, Leonid Karlinsky, James V Codella, John R Smith, Kate Saenko, Tajana Rosing, and Rogerio Feris. A broader study of cross-domain few-shot learning. In *Computer Vision—ECCV 2020: 16th European Conference, Glasgow, UK, August 23–28, 2020, Proceedings, Part XXVII 16*, pp. 124–141. Springer, 2020.
- Shell Xu Hu, Pablo G. Moreno, Yang Xiao, Xi Shen, Guillaume Obozinski, Neil D. Lawrence, and Andreas Damianou. Empirical bayes transductive meta-learning with synthetic gradients, 2020.
- Shell Xu Hu, Da Li, Jan Stühmer, Minyoung Kim, and Timothy M. Hospedales. Pushing the limits of simple pipelines for few-shot learning: External data and fine-tuning make a difference, 2022.
- Yuqing Hu, Vincent Gripon, and Stéphane Pateux. Leveraging the feature distribution in transfer-based few-shot learning, 2021.
- Kai Huang, Jie Geng, Wen Jiang, Xinyang Deng, and Zhe Xu. Pseudo-loss confidence metric for semi-supervised few-shot learning. In *Proceedings of the IEEE/CVF International Conference on Computer Vision*, pp. 8671–8680, 2021.
- Ashraful Islam, Chun-Fu Richard Chen, Rameswar Panda, Leonid Karlinsky, Rogerio Feris, and Richard J Radke. Dynamic distillation network for cross-domain few-shot recognition with unlabeled data. *Advances in Neural Information Processing Systems*, 34:3584–3595, 2021.
- Norbert Jankowski and Krzysztof Grańczewski. Universal meta-learning architecture and algorithms. *Meta-learning in computational intelligence*, pp. 1–76, 2011.
- Jinxiang Lai, Siqian Yang, Wenlong Liu, Yi Zeng, Zhongyi Huang, Wenlong Wu, Jun Liu, Bin-Bin Gao, and Chengjie Wang. tsf: Transformer-based semantic filter for few-shot learning, 2022.
- Kwonjoon Lee, Subhransu Maji, Avinash Ravichandran, and Stefano Soatto. Meta-learning with differentiable convex optimization. In *Proceedings of the IEEE/CVF conference on computer vision and pattern recognition*, pp. 10657–10665, 2019a.
- Kwonjoon Lee, Subhransu Maji, Avinash Ravichandran, and Stefano Soatto. Meta-learning with differentiable convex optimization, 2019b.
- Hongyang Li, David Eigen, Samuel Dodge, Matthew Zeiler, and Xiaogang Wang. Finding task-relevant features for few-shot learning by category traversal. In *Proceedings of the IEEE/CVF conference on computer vision and pattern recognition*, pp. 1–10, 2019a.
- Xinzhe Li, Qianru Sun, Yaoyao Liu, Shibao Zheng, Qin Zhou, Tat-Seng Chua, and Bernt Schiele. Learning to self-train for semi-supervised few-shot classification, 2019b.
- Tsung-Yi Lin, Michael Maire, Serge Belongie, James Hays, Pietro Perona, Deva Ramanan, Piotr Dollár, and C Lawrence Zitnick. Microsoft coco: Common objects in context. In *Computer Vision—ECCV 2014: 13th European Conference, Zurich, Switzerland, September 6-12, 2014, Proceedings, Part V 13*, pp. 740–755. Springer, 2014.
- Subhransu Maji, Esa Rahtu, Juho Kannala, Matthew Blaschko, and Andrea Vedaldi. Fine-grained visual classification of aircraft. *arXiv preprint arXiv:1306.5151*, 2013.

- Alex Nichol and John Schulman. Reptile: a scalable metalearning algorithm. *arXiv preprint arXiv:1803.02999*, 2(3):4, 2018.
- Alex Nichol, Joshua Achiam, and John Schulman. On first-order meta-learning algorithms. *arXiv preprint arXiv:1803.02999*, 2018.
- Jaehoon Oh, Sungnyun Kim, Namgyu Ho, Jin-Hwa Kim, Hwanjun Song, and Se-Young Yun. Understanding cross-domain few-shot learning based on domain similarity and few-shot difficulty. *Advances in Neural Information Processing Systems*, 35:2622–2636, 2022.
- Vardan Papyan, XY Han, and David L Donoho. Prevalence of neural collapse during the terminal phase of deep learning training. *Proceedings of the National Academy of Sciences*, 117(40):24652–24663, 2020.
- Cheng Perng Phoo and Bharath Hariharan. Self-training for few-shot transfer across extreme task differences. *arXiv preprint arXiv:2010.07734*, 2020.
- Alec Radford, Jong Wook Kim, Chris Hallacy, Aditya Ramesh, Gabriel Goh, Sandhini Agarwal, Girish Sastry, Amanda Askell, Pamela Mishkin, Jack Clark, et al. Learning transferable visual models from natural language supervision. In *International conference on machine learning*, pp. 8748–8763. PMLR, 2021.
- Aniruddh Raghu, Maithra Raghu, Samy Bengio, and Oriol Vinyals. Rapid learning or feature reuse? towards understanding the effectiveness of maml. *arXiv preprint arXiv:1909.09157*, 2019.
- Mengye Ren, Eleni Triantafillou, Sachin Ravi, Jake Snell, Kevin Swersky, Joshua B Tenenbaum, Hugo Larochelle, and Richard S Zemel. Meta-learning for semi-supervised few-shot classification. *arXiv preprint arXiv:1803.00676*, 2018.
- Pau Rodríguez, Issam Laradji, Alexandre Drouin, and Alexandre Lacoste. Embedding propagation: Smoother manifold for few-shot classification, 2020.
- Babak Saleh and Ahmed Elgammal. Large-scale classification of fine-art paintings: Learning the right metric on the right feature. *arXiv preprint arXiv:1505.00855*, 2015.
- Brigit Schroeder and Yin Cui. FGVCx fungi classification challenge 2018. github.com/visipedia/fgvcx_fungi_comp, 2018.
- Christian Simon, Piotr Koniusz, Richard Nock, and Mehrtash Harandi. Adaptive subspaces for few-shot learning. In *Proceedings of the IEEE/CVF conference on computer vision and pattern recognition*, pp. 4136–4145, 2020.
- Jake Snell, Kevin Swersky, and Richard Zemel. Prototypical networks for few-shot learning. *Advances in neural information processing systems*, 30, 2017a.
- Jake Snell, Kevin Swersky, and Richard S. Zemel. Prototypical networks for few-shot learning, 2017b.
- Flood Sung, Yongxin Yang, Li Zhang, Tao Xiang, Philip HS Torr, and Timothy M Hospedales. Learning to compare: Relation network for few-shot learning. In *Proceedings of the IEEE conference on computer vision and pattern recognition*, pp. 1199–1208, 2018.
- Oriol Vinyals, Charles Blundell, Timothy Lillicrap, Daan Wierstra, et al. Matching networks for one shot learning. *Advances in neural information processing systems*, 29, 2016.
- Catherine Wah, Steve Branson, Peter Welinder, Pietro Perona, and Serge Belongie. The caltech-ucsd birds-200-2011 dataset. 2011.
- Manfred K Warmuth and Dima Kuzmin. Randomized online pca algorithms with regret bounds that are logarithmic in the dimension. *Journal of Machine Learning Research*, 9(Oct):2287–2320, 2008.
- Lloyd Welch. Lower bounds on the maximum cross correlation of signals (corresp.). *IEEE Transactions on Information theory*, 20(3):397–399, 1974.

Davis Wertheimer and Bharath Hariharan. Few-shot learning with localization in realistic settings. In *Proceedings of the IEEE/CVF conference on computer vision and pattern recognition*, pp. 6558–6567, 2019.

Davis Wertheimer, Luming Tang, and Bharath Hariharan. Few-shot classification with feature map reconstruction networks, 2020.

Yibo Yang, Liang Xie, Shixiang Chen, Xiangtai Li, Zhouchen Lin, and Dacheng Tao. Do we really need a learnable classifier at the end of deep neural network? *arXiv e-prints*, pp. arXiv–2203, 2022.

Xueting Zhang, Debin Meng, Henry Gouk, and Timothy Hospedales. Shallow bayesian meta learning for real-world few-shot recognition, 2021.

A APPENDIX

A.1 SUPPLEMENTARY THEORETICAL ANALYSIS

We offer additional insight into the theoretical analysis presented in Section 4 and provide the omitted remarks, properties, lemmas, and proofs.

A.1.1 EQUIANGULAR TIGHT FRAMES

Papayan et al. (2020) coin the term Simplex Equiangular Tight Frame to describe a set of vectors $\{\phi_j\}_{j=1}^d$ such that the minimum angle between any two pairs of vectors is maximized and all vectors have equal norm. Formally,

Definition 2. Let \mathbb{R}^d be a d -dimensional inner product space over \mathbb{R} with the Euclidean inner product. A **Simplex ETF** is a set of d vectors $\{\phi_j\}_{j=1}^d$, $\phi_j \in \mathbb{R}^d$, specified by the columns of
$$\sqrt{\frac{d}{d-1}}(I_d - \frac{1}{d}\mathbb{1}\mathbb{1}^T)$$

where $I_d \in \mathbb{R}^{d \times d}$ is the identity matrix and $\mathbb{1} \in \mathbb{R}^{d \times 1}$ is the ones vector. Somewhat contradictory, a Simplex Equiangular Tight Frame is not an Equiangular Tight Frame (Welch, 1974) as this set of vectors does not form a tight frame in \mathbb{R}^d .

Definition 3. Let \mathbb{R} be a d -dimensional space over \mathbb{R} with the Euclidean inner product. An **Equiangular Tight Frame (ETF)** is a set of non-zero, equal norm vectors $\{\phi_j\}_{j=1}^n$, $n \geq d$, that achieves the Welch lower bound:

$$\max_{j \neq j'} \frac{|\langle \phi_j, \phi_{j'} \rangle|}{\|\phi_j\| \|\phi_{j'}\|} = \sqrt{\frac{n-d}{d(n-1)}}$$

It is well-known that a set of non-zero equal-norm vectors satisfies the Welch lower bound if and only if that set of vectors is equiangular and also a tight frame for \mathbb{R}^d (Fickus et al., 2018).

Definition 4. A set of non-zero, equal norm vectors $\{\phi_j\}_{j=1}^n$ is **equiangular** if $\forall j \neq j', |\langle \phi_j, \phi_{j'} \rangle| = c$ for some $c \in \mathbb{R}$, $c > 0$.

Definition 5. $\{\phi_j\}_{j=1}^n$ is a **tight frame** for \mathbb{R}^d if, $\forall v \in \mathbb{R}^d$, $\exists A > 0$ such that $A\|v\|^2 = \sum_{j=1}^n |\langle \phi_j, v \rangle|^2$.

Remark 1. A Simplex Equiangular Tight Frame is not a tight frame.

Proof. Observe that for any finite d , for $\{\phi_j\}_{j=1}^d$ equal to the columns of $\sqrt{\frac{d}{d-1}}(I_d - \frac{1}{d}\mathbb{1}\mathbb{1}^T)$, it is the case that $\sum_{j=1}^{d-1} \phi_j = -1 * \phi_d$. So $\{\phi_j\}_{j=1}^d$ do not span \mathbb{R}^d , and therefore, cannot be a tight frame. \square

Similarly, a Simplex ETF is not a d -simplex.

Remark 2. A Simplex Equiangular Tight Frame is not a simplex.

Proof. A simplex in \mathbb{R}^n requires $n + 1$ points. \square

To align terminology with properties, we generalize a Simplex ETF to an ELMES in Definition 1: a set of d vectors in a $(d + k)$ -dimensional ambient space with $k \geq 0$. Observe that a regular simplex is a special type of ETF in which the number of vectors in the set is one more than the dimension of the space that they span (Fickus et al., 2018). Building on this observation, an intuitive view of ELMES is a regular d -simplex immersed in \mathbb{R}^{d+k} .

Remark 3. Consider a centered d -dimensional regular simplex with vertices $\{\phi_j\}_{j=1}^{d+1}$, $\phi_j \in \mathbb{R}^{d+1}$. Let ι_{can} be the canonical inclusion map: $\mathbb{R}^d \rightarrow \mathbb{R}^{d+1}$, $\iota_{can}(x_1, x_2, \dots, x_d) = (x_1, x_2, \dots, x_d, 0_{d+1})$, then $\{\iota_{can}(\phi_j)\}_{j=1}^{d+1}$ is an ELMES.

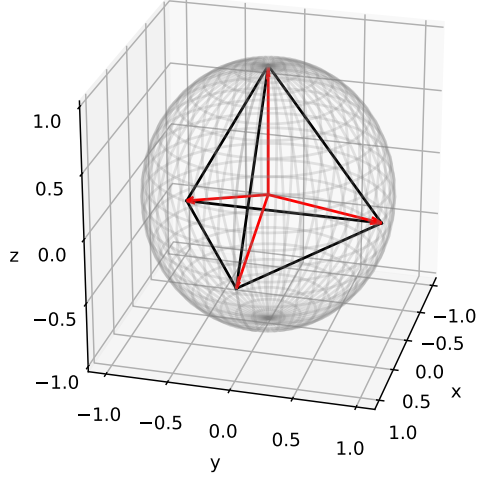


Figure 3: A visualization of a $d = 4$ ELMES in \mathbb{R}^3 . Observe the endpoints of the vectors of an ELMES lie on the vertices of a centered regular tetrahedron.

Proof. The two criteria of an ELMES are maximally equiangular and equal length. As all vertices of a centered regular d -simplex are equal length from the origin, $\{\phi_j\}_{j=1}^{d+1}$ are equal length and therefore $\{\iota_{can}(\phi_j)\}_{j=1}^{d+1}$ must also have equal length.

Similarly, from Lemma 10 of Papyan et al. (2020), we know the cosine of the angle between any two vectors in a $(d + 1)$ -dimensional ELMES is $\frac{-1}{d}$. It is known that for a d -dimensional regular simplex in \mathbb{R}^d centered at the origin, the angle subtended by any two vertices through the origin is $\cos(\theta) = \frac{-1}{d}$. Immersing $\{\phi_j\}_{j=1}^{d+1}$, $\phi_j \in \mathbb{R}^d$, into \mathbb{R}^{d+1} via the canonical inclusion operator ι_{can} does not change the pairwise angle between vectors in this set: $\langle \phi_j, \phi_{j'} \rangle = \langle \iota_{can}(\phi_j), \iota_{can}(\phi_{j'}) \rangle$. As $\{\iota_{can}(\phi_j)\}_{j=1}^{d+1}$ are equal length and maximally equiangular, it forms an ELMES. \square

We now show that an ELMES immersed in a higher dimension remains an ELMES. Taken with Remark 3, we can view a high-dimensional ELMES in \mathbb{R}^d composed of $n + 1$ vectors $\{\phi_j\}_{j=1}^{n+1}$, $d \gg n + 1$, as simply a n -simplex immersed in \mathbb{R}^d via the canonical inclusion operator.

Lemma 3. Let $\iota_{can} : \mathbb{R}^d \rightarrow \mathbb{R}^{d+k}$. If $\{\phi_j\}_{j=1}^n$ is an ELMES, then $\{\iota_{can}(\phi_j)\}_{j=1}^n$ is an ELMES.

Proof. This reduces to proving that the maximum angle between a set of d equiangular points in \mathbb{R}^d is the maximum angle between a set of d equiangular points in \mathbb{R}^{d+k} . Let $\{\phi_j\}_{j=1}^d$ be an ELMES such that $\phi_j \in \mathbb{R}^d$ and $\{\psi_j\}_{j=1}^d$ be an ELMES such that $\psi_j \in \mathbb{R}^{d+k}$. Then $\{\psi_j\}_{j=1}^d$ lie in a d -dimensional subspace of \mathbb{R}^{d+k} : $\exists \gamma_1, \dots, \gamma_d$ and basis vectors e_1, \dots, e_d such that $\forall \psi_j \in \{\psi_j\}_{j=1}^d$, $\psi_j = \sum_{i=1}^d \gamma_i e_i$. Therefore, $\forall j \neq j'$, $\langle \psi_j, \psi_{j'} \rangle \leq \langle \phi_j, \phi_{j'} \rangle$ as $\{\phi_j\}_{j=1}^d$ are an ELMES for \mathbb{R}^d . \square

A.1.2 ELMES ROTATIONAL SYMMETRY

There are infinitely many ELMES by rotating one such set of vectors about the origin.

Remark 4. Let $\{\phi_j\}_{j=1}^d$ be an ELMES in \mathbb{R}^{d+k} for some $k \geq 0$. Let $o : \mathbb{R}^{d+k} \rightarrow \mathbb{R}^{d+k}$ be an operator from the special orthogonal group $SO(d+k)$. Then $\{o(\phi_j)\}_{j=1}^d$ is also an ELMES.

Proof. Length is preserved as operations in $SO(d+k)$ have determinant 1 and angles are similarly preserved as operations in $SO(d+k)$ are unitary (i.e. preserving inner product). \square

A.1.3 A SET OF ORTHONORMAL BASIS VECTORS IS NOT AN ELMES

A final remark relates to the common misconception that a set of orthonormal basis vectors $\{\psi_j\}_{j=1}^d$ is an ELMES. While $\{\psi_j\}_{j=1}^d$ is an ETF in \mathbb{R}^d since this set realizes the Welch lower-bound in Definition 3, these vectors are not maximally equiangular: $\langle \psi_j, \psi_{j'} \rangle = 0 > \frac{-1}{d-1}$.

A.2 ELMES MAXIMIZES $p_j(X = j)$

Justification of Assumption 1. This property is implied by symmetry in the assignment of class embeddings to support classes. As the assignment is arbitrary, all learnable ψ_i class detectors should have equal probability of detecting their respective class. \square

Justification of Assumption 2. Informally, this property states that, for any m -subset of classes $\{\phi_j\}_{j=1}^m$, the probability of ψ_j detecting class j is equal to the probability of ψ_i detecting class i . This is again implied by symmetry in the assignment of class embeddings to support classes as meta-learning algorithms may predict among a subset of m classes in the support set rather than the maximum number of classes d . \square

Justification of Assumption 3. Recall in \mathbb{R}^d , $\langle \psi, \phi \rangle = \|\psi\| \|\phi\| \cos(\theta)$ where θ is the angle between ψ_i and ϕ_i . Then this assumption constrains our set $\{\phi_j\}_{j=1}^d$ so that relative norm of ϕ_i with respect to ϕ_j is lower bounded by $\cos(\theta_{i,j})$: $\frac{\|\phi_i\|}{\|\phi_j\|} > \cos(\theta_{i,j})$.

Informally, the $\{\phi_j\}_{j=1}^d$ are sufficiently spread out in the ambient space so that the learnable ψ_i that maximizes $p_i(X = i)$ is ϕ_i itself: $\psi_i = \frac{\phi_i}{\|\phi_i\|}$. This constraint helps us avoid degenerative cases similar to the $\{\phi_j\}_{j=1}^d$ all equal maximum entropy case described earlier. For example, $\phi_j = \alpha \phi_i$, $i \neq j$ with $\alpha > 0$ is one such degenerative case where one class embedding vector is stacked on a different class embedding, but with higher norm. \square

Proof of Theorem 1. Taken with Assumption 1, Assumption 2, and Assumption 3, it suffices to show Theorem 2 and Lemma 6 to prove Theorem 1. \square

Theorem 2. $p_1(X = 1) = p_2(X = 2) = \dots = p_d(X = d) \iff \{\phi_j\}_{j=1}^d$ are equiangular and equal norm.

To show the forward (\Rightarrow) direction, it suffices to first show $p_1(X = 1) = p_2(X = 2) = \dots = p_d(X = d) \Rightarrow \{\phi_j\}_{j=1}^d$ are equal norm and then show $p_1(X = 1) = p_2(X = 2) = \dots = p_d(X = d) \Rightarrow \{\phi_j\}_{j=1}^d$ are equiangular.

Lemma 4. $p_1(X = 1) = p_2(X = 2) = \dots = p_d(X = d) \Rightarrow \{\phi_j\}_{j=1}^d$ are equal norm.

Proof. This implication holds when $d = 2$:

$$\begin{aligned} p_1(X = 1) &= \frac{e^{\|\phi_1\|}}{e^{\|\phi_1\|} + e^{\|\phi_2\| \cos(\theta_{1,2})}} = \frac{e^{\|\phi_2\|}}{e^{\|\phi_2\|} + e^{\|\phi_1\| \cos(\theta_{1,2})}} = p_2(X = 2) \\ e^{\|\phi_1\|} (e^{\|\phi_2\|} + e^{\|\phi_1\| \cos(\theta_{1,2})}) &= e^{\|\phi_2\|} (e^{\|\phi_1\|} + e^{\|\phi_2\| \cos(\theta_{1,2})}) \\ e^{\|\phi_1\| + \|\phi_1\| \cos(\theta_{1,2})} &= e^{\|\phi_2\| + \|\phi_2\| \cos(\theta_{1,2})} \\ \|\phi_1\| (1 + \cos(\theta_{1,2})) &= \|\phi_2\| (1 + \cos(\theta_{1,2})) \\ \|\phi_1\| &= \|\phi_2\| \end{aligned}$$

Suppose $d > 2$ and $p_1(X = 1) = \dots = p_d(X = d)$. By Assumption 2, all m -combinations $\binom{d}{m}$ of $\{p_1(X = 1), \dots, p_d(X = d)\}$ are equal. This implies all 2-combinations are equal: $p_i(X = i) = p_j(X = j) \Rightarrow \|\phi_i\| = \|\phi_j\|$. Therefore, $\|\phi_1\| = \dots = \|\phi_d\|$. \square

Lemma 5. $p_1(X = 1) = p_2(X = 2) = \dots = p_d(X = d) \Rightarrow \{\phi_j\}_{j=1}^d$ are equiangular.

Proof. This implication is trivially true when $d = 2$ (see the proof of Lemma 4), and we show it is similarly true when $d = 3$. Following the steps in the proof of Lemma 4, we arrive at the following 3 pairs of equalities:

$$\begin{aligned} (1) \quad & e^{\|\phi_1\|(1+\cos(\theta_{1,2}))} + e^{\|\phi_1\|+\|\phi_3\|\cos(\theta_{2,3})} = e^{\|\phi_2\|(1+\cos(\theta_{1,2}))} + e^{\|\phi_2\|+\|\phi_3\|\cos(\theta_{1,3})} \\ (2) \quad & e^{\|\phi_1\|(1+\cos(\theta_{1,3}))} + e^{\|\phi_1\|+\|\phi_2\|\cos(\theta_{2,3})} = e^{\|\phi_3\|(1+\cos(\theta_{1,3}))} + e^{\|\phi_3\|+\|\phi_2\|\cos(\theta_{1,3})} \\ (3) \quad & e^{\|\phi_2\|(1+\cos(\theta_{2,3}))} + e^{\|\phi_2\|+\|\phi_1\|\cos(\theta_{1,3})} = e^{\|\phi_3\|(1+\cos(\theta_{2,3}))} + e^{\|\phi_3\|+\|\phi_1\|\cos(\theta_{1,2})} \end{aligned}$$

From Lemma 4, $p_1(X = 1) = p_2(X = 2) = p_3(X = 3) \Rightarrow \|\phi_1\| = \|\phi_2\| = \|\phi_3\|$, so the above pairs of equalities reduce to:

$$\begin{aligned} (1) \quad & \cos(\theta_{2,3}) = \cos(\theta_{1,3}) \\ (2) \quad & \cos(\theta_{2,3}) = \cos(\theta_{1,3}) \\ (3) \quad & \cos(\theta_{1,3}) = \cos(\theta_{1,2}) \end{aligned}$$

and when $d = 3$, $\{\phi_j\}_{j=1}^3$ are equiangular.

Suppose $d > 3$ and $p_1(X = 1) = \dots = p_d(X = d)$. By Assumption 2, all m -combinations $\binom{d}{m}$ of $\{p_1(X = 1), \dots, p_d(X = d)\}$ are equal. This implies all 3-combinations are equal: $p_i(X = i) = p_j(X = j) = p_k(X = k) \Rightarrow \theta_{i,j} = \theta_{i,k} = \theta_{j,k}$. Therefore, all angles are equal $\theta_{i,j} = \theta_{l,m}$ for $1 \leq i, j, l, m \leq d$. \square

Proof of Theorem 2. (\Rightarrow) Suppose $p_1(X = 1) = p_2(X = 2) = \dots = p_d(X = d)$.

By Lemma 4 and Lemma 5, $p_1(X = 1) = p_2(X = 2) = \dots = p_d(X = d) \Rightarrow \{\phi_j\}_{j=1}^d$ are equiangular and equal norm.

(\Leftarrow) Suppose $\{\phi_j\}_{j=1}^d$ are equiangular and equal norm. Let $\|\phi\|$ be the norm of any vector in our set and $\cos(\theta)$ be the pairwise angle between any two vectors. Then

$$p_i(X = i) = \frac{e^{\|\phi\|}}{e^{\|\phi\|} + (d-1)e^{\|\phi\|\cos(\theta)}} = p_j(X = j)$$

for any $1 \leq i, j \leq d$. \square

Lemma 6. For a set of equiangular and equal norm vectors, maximum equiangularity maximizes $\sum_j p_j(X = j)$.

Proof. The maximum pairwise angle between two vectors in \mathbb{R}^d is π , and from Theorem 2

$$p_i(X = i) = p_j(X = j) = \frac{e^{\|\phi\|}}{e^{\|\phi\|} + (d-1)e^{\|\phi\|\cos(\theta)}}$$

for all $1 \leq i, j \leq d$. Increasing the angle θ decreases $\cos(\theta)$. Decreasing $\cos(\theta)$ only decreases the denominator, which in turn, increases $p_i(X = i)$. Therefore, maximizing the pairwise angle between all vectors maximizes $p_i(X = i)$ for all $1 \leq i \leq d$. \square

A.2.1 AN ELMES MINIMIZES H_i

Proof of Lemma 1. Equal norm and equiangular $\{\phi_j\}_{j=1}^d$ are bounded in norm, and thus, the set of probability distributions we obtain $\{p_1, p_2, \dots, p_d\}$ belong to a capped simplex (Warmuth & Kuzmin, 2008) $\Delta_c^d = \{p \in \Delta \mid \max_i p_i \leq c\}$ where $c = \frac{e^{\|\phi\|^2}}{e^{\|\phi\|^2} + (d-1)e^{\|\phi\|^2 \cos(\theta)}}$. Clearly, among such probability vectors, the minimum entropy is achieved at the boundary where $\cos(\theta)$ is minimized, i.e., when the $\{\phi_j\}_{j=1}^d$ are maximally equiangular. \square

A.2.2 AN ELMES MAINTAINS PERMUTATION INVARIANCE

Proof of Lemma 2. This follows from row-wise equivariance to permutations in matrix multiplication. For any permutation $\pi : [1, \dots, n] \rightarrow [1, \dots, n]$ applied to the rows of \mathcal{S}^n , we have $\pi(\mathcal{S})W = \pi(\mathcal{S}W)$. \square

B ELMES ABLATION

Table 5: **CUB & tiered-ImageNet & Aircraft** mean accuracy and standard error across 10,000 test epochs.

Method	CUB		tiered-ImageNet		Aircraft	
	5w-1s	5w-5s	5w-1s	5w-5s	5w-1s	5w-5s
CAML [ELMES Class Embedding]	91.8±.2	97.1±.1	95.4±.1	98.1±.1	63.3±.3	79.1±.2
CAML [Learnable Class Embedding]	91.8±.2	97.1±.1	95.3±.1	98.3±.1	66.3±.2	80.6±.2

Table 6: **MiniImageNet & CIFAR-fs** mean accuracy and standard error.

Method	CIFAR-fs		MiniImageNet	
	5w-1s	5w-5s	5w-1s	5w-5s
CAML [ELMES Class Embedding]	70.8±.2	85.5±.1	96.2±.1	98.6±.0
CAML [Learnable Class Embedding]	71.1±.2	85.9±.1	96.1±.1	98.7±.0

Table 7: **Pascal & Paintings** mean accuracy and standard error across 10,000 test epochs.

Method	Pascal + Paintings		Paintings		Pascal	
	5w-1s	5w-5s	5w-1s	5w-5s	5w-1s	5w-5s
CAML [ELMES Class Embedding]	63.8±.2	78.3±.1	51.1±.2	65.2±.1	82.6±.2	89.7±.1
CAML [Learnable Class Embedding]	63.1±.2	78.0±.1	51.3±.2	65.0±.1	82.1±.2	89.7±.1

Table 8: **meta-iNat & tiered meta-iNat & ChestX** mean accuracy and standard error across 10,000 test epochs.

Method	meta-iNat		tiered meta-iNat		ChestX	
	5w-1s	5w-5s	5w-1s	5w-5s	5w-1s	5w-5s
CAML [ELMES Class Embedding]	91.2±.2	96.3±.1	81.9±.2	91.6±.1	21.5±.1	22.2±.1
CAML [Learnable Class Embedding]	91.4±.2	96.4±.1	82.1±.2	91.8±.1	21.5±.1	22.6±.1